Site Differentiation by Synchrotron Radiation Resonant Scattering: Case Study of $BaZn_2Ge_2$

Davide M. Proserpio,*,† Gilberto Artioli,‡ Suzanne Mulley,† Gerardo Chacon,§ and Chong Zheng*,§

Dipartimento di Chimica Strutturale e Stereochimica Inorganica and Dipartimento di Scienze della Terra, Università di Milano, I-20133 Milano, Italy, and Department of Chemistry, Northern Illinois University, DeKalb, Illinois 60115

Received November 1, 1996. Revised Manuscript Received January 27, 1997⊗

Resonance scattering was applied for the first time to the class of solids with the AB_2X_2 stoichiometry. A few members of this family seem to violate the developed rules describing the structure−property relationship, and the source of ambiguity is often the experimental determination of the structure itself. As an example, the newly synthesized $BaZn_2Ge_2$ can in principle adopt either the $ThCr_2Si_2$ or the $CaBe_2Ge_2$ type structures, and conventional diffraction techniques do not allow discrimination between the two structure models. The resonance scattering method shows, however, that $BaZn_2Ge_2$ crystallizes in the $ThCr_2Si_2$ structure (tetragonal $I4/mmm$; $a = 4.527(2)$ Å $c = 10.555(3)$ Å, $Z = 2$), in agreement with theoretical analyses.

Introduction

Nearly 600 solid-state compounds with the stoichiometric ratio AB_2X_2 (A = the alkali-metal, alkaline-earth, or rare-earth elements; B = the transition-metal elements, and X = the main-group elements) crystallize in the $ThCr_2Si_2$ structure.[1] Dozens of others adopt the related $CaBe_2Ge_2$ type.[2] Many of these compounds exhibit interesting physical properties such as superconductivity,[3] unusual magnetic behavior, valence fluctuation, or heavy fermion phenomenon,[4] and of course their physical properties are directly related to their crystal structure and crystal chemistry. For example, a superconducting transition has been observed for $LaIr_2Si_2$ crystallizing in the quenched metastable $CaBe_2Ge_2$ structure but not in the annealed, lower energy $ThCr_2Si_2$ allotrope.[5] A considerable effort has been devoted to the rationalization of the physicochemical factors determining the structural preference in terms of competition between the interlayer and the intralayer bonding interactions.[6] The balance between the two types of interactions can be suitably changed by elemental substitution. A clear example is the $BaMg_2X_2$ (X = Si, Ge, Sn, Pb) series,[7] where the heavier Sn, Pb elements favor the interlayer interaction, and therefore the $CaBe_2Ge_2$ structure, while the lighter Si, Ge elements prefer the $ThCr_2Si_2$ structure.

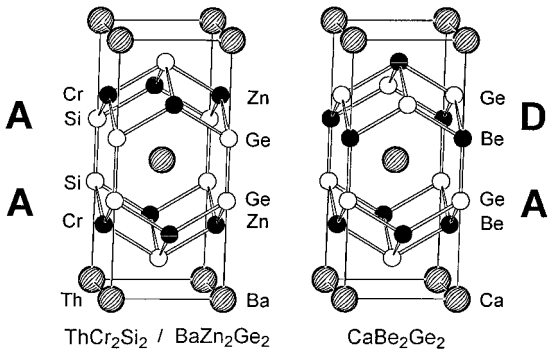

Figure 1. Crystal structure of $BaZn_2Ge_2$ of $ThCr_2Si_2$ type (left), and of $CaBe_2Ge_2$ type (right).

The intralayer and interlayer interactions are easily described by considering that the $ThCr_2Si_2$ structure (the left side of Figure 1) is made of only one type of layer (layer **A**). The $CaBe_2Ge_2$ structure, however, is built up with alternating **A** and **D** layers (right side of Figure 1). In layer **A**, the more electropositive element (such as Cr or Be) occupies the sites lying in the central plane of the layer; whereas in **D** the central sites are occupied by the more electronegative element (such as Ge or Si). The orbital overlap between the center sites

† Dipartimento di Chimica Strutturale e Stereochimica Inorganica.
‡ Dipartimento di Scienze della Terra.
§ Northern Illinois University.
⊗ Abstract published in *Advance ACS Abstracts,* March 15, 1997.

(1) Just, G.; Paufler, P. *J. Alloys Compd.* **1996**, *232*, 1. Marchant, R.; Jeitschko, W. *J. Solid State Chem.* **1978**, *24*, 351. Jeitschko, W.; Jaberg, B. *J. Solid State Chem.* **1980**, *35*, 312. Hoffmann, W. K.; Jeitschko, W. *J. Solid State Chem.* **1984**, *51*, 152. Parthé, E.; Chabot, B.; Braun, H. F.; Engel, N. *Acta Crystallogr., Sect. B* **1983**, *39*, 588. Pearson, W. B. *J. Solid State Chem.* **1985**, *56*, 278. Hulliger, F. *Helv. Phys. Acta* **1985**, *58*, 216.

(2) Eisenmann, B.; May, N.; Müller, W.; Schäfer, H. *Z. Naturforsch., B: Anorg. Chem., Org. Chem.* **1972**, *27*, 1155. Cordier, G.; Eisenmann, B.; Schäfer, H. *Z. Naturforsch., B: Anorg. Chem., Org. Chem.* **1976**, *426*, 205. Dorrscheidt, W.; Savelsberg, G.; Stöhr, J.; Schäfer, H. *J. Less-Common Met.* **1982**, *83*, 269.

(3) Shelton, R. N.; Braun, H. F.; Musik, E. *Solid State Commun.* **1984**, *52*, 797. Braun, H. F. *J. Less-Common Met.* **1984**, *100*, 105.

(4) Steglich, F.; Aarts, J.; Bredl, C. D.; Lieke, W.; Meschede, D.; Franz, W.; Schäfer, H. *Phys. Rev. Lett.* **1979**, *43*, 1892. Lieke, W.; Rauchschwalbe, U.; Bredl, C. D.; Steglich, F.; Aarts, J.; de Boer, F. R. *J. Appl. Phys.* **1982**, *53*, 2111. Assmus, W.; Herrmann, M.; Rauchschwalbe, U.; Regel, S.; Lieke, W.; Spille, H.; Horn, S.; Weber, G.; Steglich, F.; Cordier, G. *Phys. Rev. Lett.* **1984**, *52*, 469. Stewart, G. R. *Rev. Mod. Phys.* **1984**, *56*, 755. Varma, C. M. *Comments Solid State Phys.* **1985**, *11*, 221. *Theory of Heavy Fermions and Valence Fluctuations*; Kasuya, T., Saso, T., Eds.; Springer-Verlag: New York, 1985. Schlottmann, P. *Phys. Rep.* **1989**, *181*, 1. Reehuis, M.; Jeitschko, W. *J. Phys. Chem. Solid* **1990**, *51*, 961. Das, I.; Sampathkumaran, E. V.; Vijayaraghavan, R. *J. Less-Common Met.* **1991**, *171*, L13.

(5) Braun, H. F.; Engel, N.; Parthé, E. *Phys. Rev. B* **1983**, *28*, 1389. Higashi, I.; Lejay, P.; Chevalier, B.; Étourneau, J.; Hagenmuller, P. *Rev. Chim. Miner.* **1984**, *21*, 239.

(6) Zheng, C.; Hoffmann, R. *J. Am. Chem. Soc.* **1986**, *108*, 3078.

(7) Eisenmann, B.; Schäfer, H. *Z. Anorg. Allg. Chem.* **1974**, *403*, 163.

S0897-4756(96)00564-9 CCC: $14.00

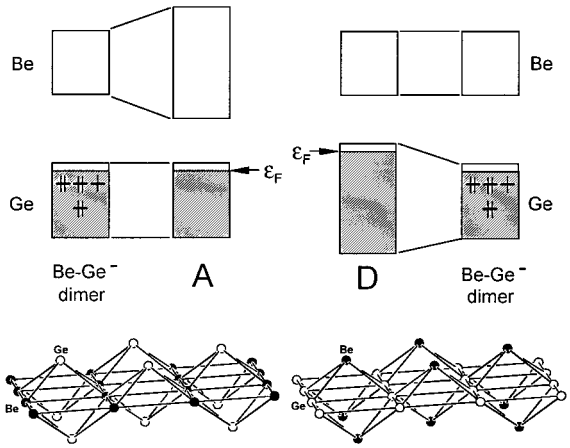

Figure 2. Graphical representation of the orbital dispersion effect due to the structural layers **A** and **D**.

is larger than between the outer sites, so that there is more band dispersion (or larger separation of the lowest and highest molecular orbitals) for the center sites. If we build up the layers using Be−Ge dimers, as in the $CaBe_2Ge_2$ type structure, layer **A** is composed of Be center sites surrounded by Ge outer atoms, whereas layer **D** has the more electronegative Ge atoms in the central layer sites. The orbitals of the Be−Ge dimer are divided into an upper block, which is mostly of the more electropositive Be character, and a lower block, which is mostly Ge orbitals. The lower block of four orbitals is almost filled with seven electrons, as the formal electron count of $Ca^{2+}(Be_2Ge_2)^{2-}$ gives a negatively charged dimer $Be-Ge^-$ (seven valence electrons). Figure 2 shows the larger dispersion of the upper orbital block in layer **A**. It is clear that the Fermi level (or HOMO) is higher in layer **D** than in layer **A** because of the difference in band dispersion. Layer **D** also contains a larger extent of antibonding character similar to that of a two-orbital four-electron repulsion.[8] Therefore in the **A**−**D** stacking the intralayer interaction favors layer **A**, while the interlayer interaction favors the donor−acceptor pattern shown in Figure 3 (bottom). The **A**−**A** stacking in the $ThCr_2Si_2$ structure introduces a two-orbital four-electron repulsion[8] shown in Figure 3 (top). As the principal quantum number increases in element X, the intralayer interaction diminishes because of a more diffused orbital and poorer overlap. Thus $BaMg_2Si_2$ adopts the $ThCr_2Si_2$ structure, whereas $BaMg_2Pb_2$ crystallizes in the $CaBe_2Ge_2$ structure type.

The $BaMg_2X_2$ (X = Si, Ge, Sn, Pb) series is the only one that has been synthesized for all four elements.[7] $BaZn_2X_2$ is another interesting series yet to be studied: $BaZn_2Sn_2$ crystallizes in the $CaBe_2Ge_2$ structure type,[2] while theoretical calculations indicate that $BaZn_2Ge_2$ should assume the $ThCr_2Si_2$ structure, although no synthesis has been reported for $BaZn_2Ge_2$ to date.

Experimental Section

Synthesis. The synthesis was carried out by mixing elemental Ba, Zn, and Ge in a stoichiometric ratio and wrapping the mixture in a Ta foil and placing the capsule in a carbon-black coated quartz ampule, so to protect the quartz ampule from corrosion by Ba. The ampule was then sealed under a vacuum of 10^{-4} Torr, heated in a computer-controlled furnace to 1220 °C in 15 h, and kept at the reaction temperature for 168 h before annealing to room temperature in 96 h. Powder X-ray diffraction analysis on the final product indicated a ca. 10% yield with the rest of the sample being Zn and Ge and some binary phases. Several metallic single crystals of approximate size $0.1 \times 0.1 \times 0.08$ mm^3 were used for crystal structure determination.

Diffraction Data Collection and Analysis. A preliminary data collection using conventional Mo Kα radiation allowed evaluation of the tetragonal unit-cell parameters (see Tables 1 and 2), though the structure refinement using these data was unable to discriminate between the two structure models. The main problem is that the lattice ordering scheme is determined by the site distribution of Zn and Ge, which are nearly isoelectronic and produce no scattering contrast using the characteristic radiation of Mo. All reflections violating the extinction conditions corresponding to the I lattice of the $ThCr_2Si_2$ structure type are therefore very weak, and it is not possible to establish the presence of lattice violations with statistical significance. To increase the scattering contrast between the two species, additional data were collected using synchrotron X-rays at wavelengths corresponding to the absorption edge of Zn and Ge. It is well-known that the anomalous scattering in proximity to the absorption edge produces significant scattering variation because of the resonance effect.[9] In the case of Zn and Ge, the difference between the f' coefficients (the real part of the anomalous scattering correction of the scattering factors) is $f'(Ge)-f'(Zn) = -6.6$

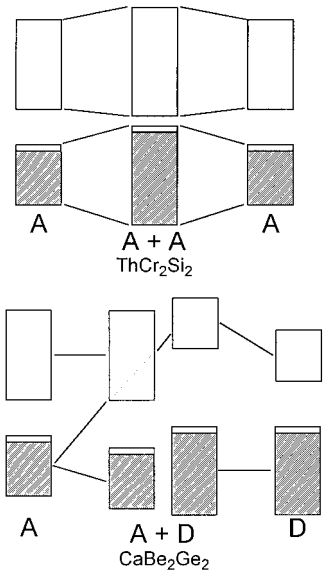

Figure 3. Donor−acceptor patterns due to the interlayer interaction of the **A**−**D** layer stacking (bottom); and two-orbital four-electron repulsion due to the **A**−**A** layer stacking (top).

Table 1. Crystallographic Data for $BaZn_2Ge_2$

formula weight	413.26	crystal system	tetragonal
space group	*I*4/*mmm* (139)	Z	2
a, Å	4.527(2)	*c*, Å	10.555(3)
V, Å^3	216.3(2)	density (calc), g cm^{-3}	6.345
temp, K	293(2)	crystal size, mm	0.1 × 0.1 × 0.08

Table 2. Atomic Coordinates and Equivalent Isotropic Displacement Parameters (Å^2) for $BaZn_2Ge_2$[a]

	x	y	z	*U*(eq)
Ba	0	0	0	0.0049(7)
Zn	0	1/2	1/4	0.0085(10)
Ge	0	0	0.3787(2)	0.0081(9)

[a] *U*(eq) is defined as one-third of the trace of the orthogonalized U_{ij} tensor.

(8) Albright, T. A.; Burdett, J. K.; Whangbo, M. *Orbital Interactions in Chemistry*; Wiley: New York, 1985.

(9) Cox, D. E.; Wilkinson, A. P. *Resonant anomalous X-ray scattering theory and applications*; North-Holland: Amsterdam, 1994.

Table 3. Refined Real Coefficents ($\Delta f'$) of the Anomalous Part of the Scattering Factors for Each Individual Data Set

	atom type		
data set	Ba	Zn	Ge
1	−0.312	−2.21(17)	−7.78(22)
2	−0.512	−8.92(21)	−3.39(21)
4	−0.312	−2.44(13)	−6.62(14)
5	−0.512	−8.13(22)	−3.44(18)

electrons at the Ge K absorption edge (11.103 keV), and it is $f'(Ge) - f'(Zn) = +6.1$ electrons at the Zn K absorption edge (9.659 keV). These differences correspond to the scattering contrast between the chemical species gained by tuning at the resonant wavelengths. The values above are based on the f' coefficients for free neutral atoms computed by self-consistent field relativistic Dirac−Slater wave functions[10] and do not take into account of the fine-structure oscillations due to the chemical environment of the bonded atoms in the structure. The experimentally observed f' coefficients are therefore expected to deviate slightly from the calculated values, though the effect is known to be small compared to the contrast gain.

The diffraction data were collected at the materials science wiggler beamline (BL2) of the European Synchrotron Radiation Facility (ESRF) in Grenoble, France, using a Siemens SMART CCD area detector system. The Si(111) monochromator was carefully calibrated at the Zn and Ge K absorption edges by measuring the edge on metallic Zn and Ge foils and by selecting the positions at half the edge jump. Two crystals from the same synthesis batch were measured at both wavelengths, for a total of 278 observed intensities. The data were added to the 186 observed reflections collected with conventional Mo radiation and simultaneously refined against a unique structural model using the GSAS package.[11] The multiwavelength structural refinement using 426 reflections above the 3σ level straightforwardly converged to an overall residual factor $Rw(F) = 0.072$ for the model adopting the $I4/mmm$ $ThCr_2Si_2$ structure type, while no convergence at all was reached for the model in the $P4/nmm$ $CaBe_2Ge_2$ structure type. Despite the relatively high residual factors ($Rw(F)$ in the range 0.039−0.157 for the single data sets) caused by the nonideal quality of the crystals and by the low signal/noise ratio of the detector setting, the structural refinement using the overdetermined observations allowed straightforward simultaneous refinement of atomic coordinates, site anisotropic displacement parameters, site occupancy factors (unconstrained to full site occupancy), and f' coefficients.

The anomalous scattering coefficients were independently and freely refined for each data set (see Table 3), permitting slight missettings of the monochromator for different data collections. The refined absolute f' values are all systematically lower than the theoretically computed values by about one electron, clearly indicating near-edge EXAFS oscillations effects, though the relative differences are in excellent agreement with those calculated above ($f'(Ge) - f'(Zn) = -5.6$ and +5.5 electrons at the Ge and Zn edges, respectively). Given the straightforward and unambiguous solution that the resonant scattering experiment has provided to our structural problem, it is somehow surprising that the technique has been applied only in a limited number of crystal structural analyses, though recently it has received new pulse by the development of DAFS (diffraction anomalous fine structure) and DANES (diffraction anomalous near-edge structure) experimental methods.[12]

Computational Details. The extended Hückel tight binding parameters used in the simulations are listed in Table 4.[13]

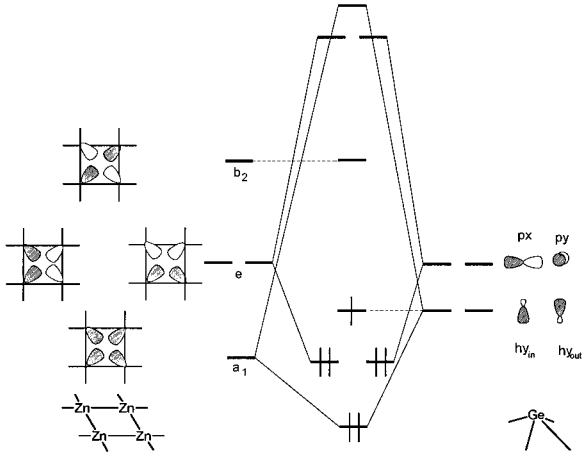

Figure 4. Graphical representation of the intralayer interaction.

Table 4. Extended Hückel Parameters

	orbital	H_{ii} (eV)	ζ	ref
Ba	6s	−7.0	1.2	15
	6p	−4.0	1.2	
Ge	4s	−16.0	2.16	16
	4p	−9.0	1.85	
Zn	4s	−12.41	2.01	17
	4p	−6.53	1.70	

A set of 108K points generated using the method of Pack and Monkhorst[14] was used for the COOP calculations.

Results and Discussion

The tetragonal $BaZn_2Ge_2$ structure is shown on the left side of Figure 1, with Cr,Si substituted by Zn,Ge; see also Table 5. The shortest Zn−Ge distance is 2.640(2) Å, a little longer than the sum of the covalent radii of Zn (1.25 Å) and Ge (1.22 Å) but much shorter than the sum of the ionic radii of Zn^{2+} (0.60 Å) and Ge^{4-} (2.72 Å).[18] Thus the Zn−Ge bond can be characterized as covalent. The interlayer Ge−Ge bond of 2.559(6) Å is slightly longer than the Ge−Ge bond (2.45 Å) in the elemental diamond structure of Ge.[19] Both distances are comparable with those observed in the isotypic compounds $CaZn_2Ge_2$[20] and $SrZn_2Ge_2$.[21] Zn is at the center of a Ge_4 tetrahedron, and the tetrahedra extend into two-dimensional layers by edge-sharing. The Ba atoms are positioned above and below the niches of the tetrahedral layers. Having 14 valence electrons, the electronic structure of $BaZn_2Ge_2$ is similar to the one of $BaAl_4$, and the bonding pattern is related to that of B_5H_9.[22] The intralayer interaction is summarized in Figure 4.

(10) Cromer, D. L. *Acta Crystallogr.* **1965**, *18*, 17.
(11) GSAS *Generalised Structure Analysis System;* Larson, A. C.; Von Dreele, R. B. Document LAUR 86-748, Los Alamos National Laboratory, Los Alamos, NM.
(12) Vacinova, J.; Hodeau, J. L.; Wolfers, P.; Lauriat, J. P.; Elkaim, E. *J. Synchr. Radiat.* **1995**, *2*, 236. Hodeau, J. L.; Vacinova, J. *Synchr. Radiat. News* **1996**, *9*, 15.
(13) Hoffmann, R.; Lipscomb, W. N. *J. Chem. Phys.* **1962**, *36*, 2179. Hoffmann, R.; Lipscomb, W. N. *J. Chem. Phys.* **1962**, *37*, 2872. Hoffmann, R. *J. Chem. Phys.* **1963**, *39*, 1397. Whangbo, M.-H.; Hoffmann, R.; Woodward, R. B. *Proc. R. Soc. London* **1979**, *A366*, 23.
(14) Pack, J. D.; Monkhorst, H. J. *Phys. Rev. B* **1977**, *16*, 1748.
(15) Zheng, C. *J. Am. Chem. Soc.* **1993**, *115*, 1047.
(16) Thorn, D. L.; Hoffmann, R. *Inorg. Chem.* **1978**, *17*, 126.
(17) Silvestre, J.; Albright, T. A. *Isr. J. Chem.* **1983**, *23*, 139.
(18) Pauling, L. *The Nature of the Chemical Bond*; Cornell University Press: Ithaca, NY, 1960.
(19) Donohue, J. *The Structures of the Elements*; Krieger: Malabar, FL, 1982.
(20) Eisenmann, B.; May, N.; Müller, W.; Schäfer, H.; Weiss, A.; Winter, J.; Ziegleder, G. *Z. Naturforsch. B: Anorg. Chem., Org. Chem.* **1970**, *25*, 1350.
(21) Dörrscheidt, W.; Niess, N.; Schäfer, H. *Z. Naturforsch. B: Anorg. Chem., Org. Chem.* **1976**, *31*, 890.
(22) Lipscomb, W. N. *Boron Hydrides*; Benjamin: New York, 1963.

Table 5. Selected Bond Lengths [Å] and Angles [deg] for $BaZn_2Ge_2$

Zn−Ge × 4	2.640(2)	Ba···Ge × 8	3.447(2)	Ba···Zn × 4	3.4766(9)
Ge−Ge	2.559(6)	Ge−Zn−Ge × 4	105.37(5)	Ge−Zn−Ge × 2	118.03(12)

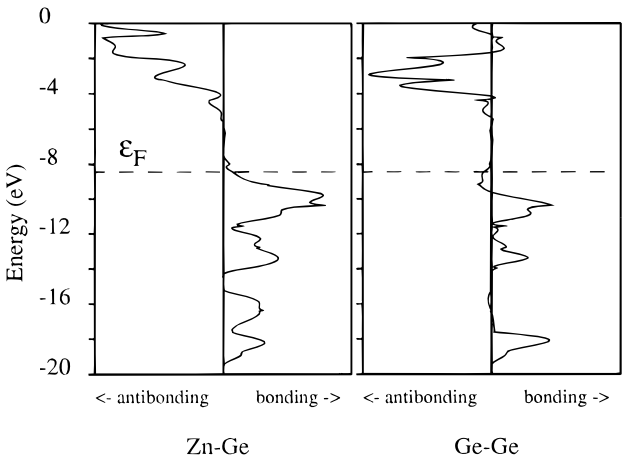

Figure 5. Crystal orbital overlap population curves for the intralayer Zn−Ge (solid line) and interlayer Ge−Ge (dotted line) bonds.

Each Ge atom is above a hollow of the Zn square lattice. Each of the four Zn atoms forming the hollow contribute an sp^3 hybrid, and the four sp^3 hybrids form an a_1, two e, and one b_2 molecular orbitals ready to interact with the Ge orbitals. The Ge atom can form two sp hybrids, one pointing toward the hollow (hy_{in}), and one pointing away (hy_{out}), and it also has two p orbitals (p_x, p_y). The hy_{in} hybrid interacts with the a_1 orbital because it has the same symmetry pattern. Similarly, p_x and p_y combine with the e orbitals, and the hy_{out} and b_2 orbitals have no matching orbitals to interact. These are thus nonbonding. However, the hy_{out} orbital can form a σ and a σ^* orbitals with another hy_{out} in the adjacent layer. When the bonding a_1, e and σ orbitals are filled, the solid achieves maximum bonding. The electron count for this is 7 per hollow, with the a_1, the doubly degenerate e, and σ orbitals occupied. Since the σ orbital is shared between two layers, each hollow needs to contribute only one electron. Since each hollow (needing seven electrons) contains only one Zn and one Ge, the electron count corresponding to maximum bonding for $BaZn_2Ge_2$ is 14. Figure 5 shows the computed crystal orbital overlap population (COOP)[23] curves for the intralayer Zn−Ge and the interlayer Ge−Ge bonds, using the extended Hückel tight binding method. Indeed, below the Fermi level corresponding to the electron count of 14, all states contribute to bonding. The COOP curve is actually the overlap population weighted by the density of states, plotted in increasing energy, and the positive values indicate that the states in a particular energy range contribute to bonding.

An extended Hückel calculation has also been performed for a hypothetical $BaZn_2Ge_2$ compound in the $CaBe_2Ge_2$ framework. The lattice parameters are taken from the actual crystal structure of $BaZn_2Ge_2$ except that the Zn and Ge positions are inverted in alternating layers. A comparison of the two possible structures is shown in Table 6.

(23) Hoffmann, R. *Angew. Chem., Int. Ed. Engl.* **1982**, *21*, 711.

Table 6. Calculated Bond and Madelung Energies of $BaZn_2Ge_2$ Adopting the $ThCr_2Si_2$ and $CaBe_2Ge_2$ Structures

structural type	bond energy (eV)	Madelung energy (eV)
$ThCr_2Si_2$	−362.7	−9.0
$CaBe_2Ge_2$	−361.4	−14.2

The $ThCr_2Si_2$ type have lower bond energy than the $CaBe_2Ge_2$ type because of the bonding pattern described in Figure 2. Indeed, the computed overlap populations for the Zn−Ge bond in the $ThCr_2Si_2$ layer type (0.447) and in layer type **D** of the $CaBe_2Ge_2$ (0.405) show that the bond is weaker in the latter. However, the Madelung energy favors the $CaBe_2Ge_2$ type, as this structure contains alternating positively charged donor and negative charged acceptor layers. The Madelung contribution was calculated using the Mulliken charges obtained by the extended Hückel method, and the Ewald sum was used to ensure the convergence.[15] The vacuum dielectric constant was used, and the computed energy values are therefore likely to be overestimated.

This case study represents a textbook example of a relatively simple structure for which the correct structural prediction based on the systematic theoretical analysis of isostructural compounds is available. Nonetheless for the title compound energy calculations proved to be either misleading, as in the case of the Madelung energy computation, or hardly conclusive, as in the case of the extended Hückel calculation where the resulting energy values are insensitive to the structural model. More sophisticated computational tecniques will be tried in the future. Furthermore, the full structural characterization of the specific compound is impossible with conventional diffraction methods. Only with the use of synchrotron resonant scattering can the structure be solved without ambiguity. Moreover, in our case, the enhancement of scattering contrast by neutron diffraction is not viable, because of the very limited quantity of synthesized sample. Neutron diffraction at present requires a much larger quantity of diffracting sample. We believe that this powerful technique can be advantageously extended to the structure analysis of a large number of compounds for which the structural solution is troublesome with conventional techniques.

Acknowledgment. This work has been supported in part by NSF through the Presidential Young Investigator program (CHE-91-57717) and by the donors of the Petroleum Research Fund, administered by the American Chemical Society. Dr. Åke Kvick of ESRF is thanked for help during synchrotron data collection. Italian CNR and MURST are acknowledged for funding.

Supporting Information Available: Full list of data collection parameters, structure refinement details, atomic coordinates, and anisotropic displacement parameters (3 pages); observed and calculated structure factors (2 pages). Ordering information is given on any current mashead page.

CM960564V